Journal of
Synchrotron
Radiation

ISSN 0909-0495

Received 1 March 2012
Accepted 6 June 2012

Simultaneous measurement of X-ray diffraction and ferroelectric polarization data as a function of applied electric field and frequency

Jenny Wooldridge,[a]* Steph Ryding,[b] Simon Brown,[c,d] Tim L. Burnett,[a] Markys G. Cain,[a] Robert Cernik,[b] Ricardo Hino,[e] Mark Stewart[a] and Paul Thompson[c,d]

[a]National Physical Laboratory, Hampton Road, Teddington TW11 0LW, UK, [b]Manchester Materials Science Centre, Grosvenor Street, Manchester M13 9PL, UK, [c]XMaS, The UK CRG, ESRF, BP 220, F-38043 Grenoble Cedex, France, [d]University of Liverpool, Liverpool L69 3BX, UK, and [e]ESRF, BP 220, F-38043 Grenoble Cedex, France. E-mail: jenny.wooldridge@npl.co.uk

The characteristics of a new ferroelectric measurement system at the European Synchrotron Radiation Facility are presented. The electric-field-induced phase transitions of $Pb(Mg_{1/3}Nb_{2/3})O_3$–$xPbTiO_3$ are determined *via in situ* measurements of electric polarization within the synchrotron diffraction beamline. Real-time data collection methods on single-crystal samples are employed as a function of frequency to determine the microstructural origin of piezoelectric effects within these materials, probing the dynamic ferroelectric response.

Keywords: ferroelectric; polarization; dynamic; *in situ*; X-ray diffraction.

1. Introduction

Relaxor ferroelectrics (RFEs) are of technological importance for many applications including sonar, transducers, energy harvesting devices and memory storage (Park & Hackenberger, 2002). Most commercial materials are perovskites with morphotropic phase boundary (MPB) compositions, where solid solutions of the same prototype structure but with different structural distortions are separated by an almost vertical, or temperature-independent, phase boundary in the chemical phase diagram. According to the Web of Knowledge Service, the citation rate of papers investigating the properties of RFEs at the MPB has increased tenfold in the past decade, matching the rapid increase in their use in applications. In the continual drive to optimize device performance through materials engineering, a thorough understanding of the origins of the high piezoelectric and dielectric coefficients in these materials is required. Both are strongly correlated with the crystal structure (Bokov & Ye, 2006), and so there have been many recent diffraction studies (Daniels *et al.*, 2007; Ye *et al.*, 2003; Singh *et al.*, 2006) aiming to provide the link between microscopic and macroscopic functional materials properties.

Studies of the electric-field-induced phase transitions in RFEs materials have focused on structural refinements through X-ray and/or neutron diffraction under applied DC electric fields, for example Bai *et al.* (2004). The microscopic origin of the piezoelectric properties is then inferred by comparison with polarization and strain data measured in separate experiments, for example Davis *et al.* (2006). The crystal structure in RFEs around the MPB is highly sensitive to chemical composition, temperature, stress and electric field (McLaughlin *et al.*, 2004). In addition to this, the relaxor nature of these materials results in the history of poling conditions and electrical loading having a significant effect on phase composition and microstructure (Chen *et al.*, 2002; Zhao *et al.*, 2002). For these reasons, comparisons between the crystallography and ferroelectric polarization is only possible when they are measured simultaneously, on the same sample. The motion of domain walls contributes greatly to the performance of these materials (Ye & Dong, 2000), and consequently crystallographic measurements need to be extended into the time domain, at frequencies within the operational range of applications using RFEs. In this paper we present a new measurement system which can simultaneously record X-ray diffraction and polarization data as a function of applied AC electric fields. This way, the *in situ* link between the structural and functional properties of the ferroelectric materials can be more rigorously explored.

The pioneering work of Shrout and co-workers (Park & Shrout, 1997) has shown that it is possible to exploit a maximal piezoelectric response by the use of domain engineering and appropriate crystal cuts in single crystals. It is possible to grow large crystals of $Pb(Mg_{1/3}Nb_{2/3})O_3$–$xPbTiO_3$ (PMN–PT) and $Pb(Zn_{1/3}Nb_{2/3})O_3$–$xPbTiO_3$ (PZN-PT) with MPB compositions, and to realise piezoelectric properties that are almost an order of magnitude greater than those achievable with polycrystalline piezoelectric ceramics, such as $Pb(Zr_{1-x}Ti_x)O_3$ (PZT).

The electric-field-induced transformations in PMN–PT are not yet fully understood. It is traditionally thought that the

high piezoelectric coefficients in these materials are due to the existence of one or more of the monoclinic phases, in which the polar vector is confined to one of three planes. A large change in polarization is achievable with modest electric fields because the crystal is able to utilize these 'bridging' phases in order to transform from a rhombohedral to tetragonal orientation, or *vice versa*. However, in recent years the existence of the monoclinic phases has been questioned: the same macroscopic symmetry could be inferred by finely twinned R and T domains, piezoelectric distortions on these higher symmetry phases, or even a chemical order–disorder transition, all of which would present the same evidence in an X-ray or neutron diffraction experiment (Davis, 2007). We leave the interpretation of the physical significance of our results for future publications, and in this paper discuss the technicalities of performing the experiments using this new beamline measurement system.

1.1. Experimental approach

The direction of the internal electrical polarization (P) of a ferroelectric can be switched by the application of an external electric field (E), and the usual method of identifying and characterizing a ferroelectric material is to map the hysteretic relationship between these two parameters, known as a PE loop. In order to use X-ray diffraction to investigate this dynamic switching process, time-resolved data need to be captured. The key to developing a useful experimental set-up is to accurately synchronize the timing between the diffraction and polarization data collection as a function of the applied electric field. Only when this has been achieved is it possible to interpret the structural transformations that correspond to an applied electric field around the PE loop, and how these relate to the functional behaviour of the material.

We have developed a beamline *in situ* PE loop system which makes these measurements possible, at the European Synchrotron Radiation Facility (ESRF, Grenoble, France), for measurements on single-crystal samples. A detailed description of the experimental set-up and the results that can be achieved is presented.

1.2. Measurement challenges

The metrology associated with a PE loop measurement is purely electrical, and, whilst this is important for many applications, there are instances in which the polarization-induced mechanical strain is of major interest, in actuators for example. This strain is a reflection of electric-field-induced unit-cell structural changes and ferroelectric domain wall motion within the material. In order to understand this behaviour at a fundamental level, it is important to probe these atomic structural changes using X-ray or other diffraction methods. Typically, this involves measuring the diffraction pattern under an applied DC electrical field (Schonau *et al.*, 2007; Hinterstein *et al.*, 2011), and, whilst this does give some insight into the mechanisms taking place, the dynamic aspects of the process are not recorded. Although the PE loop does not contain any time information, it is nevertheless a dynamic measurement and is often strongly frequency dependent (Waser *et al.*, 2005). The synchronous determination of dynamic and structural phenomena presents a temporal challenge since the diffraction data collection time is often an order of magnitude longer than the electrical measurement time. Our new measurement system described in §2.2 allows for the measurement of real-time polarization and diffraction data over a range of electrical field frequencies. Whilst some dynamic *in situ* measurements have been reported elsewhere (Jones *et al.*, 2006; Daniels *et al.*, 2007; Pramanick *et al.*, 2010; Moriyoshi *et al.*, 2011), these studies employed stroboscopic techniques to allocate diffraction patterns to electrically switched polarization states. We have found that, with real-time measurements, effects such as polarization fatigue and drift of the field values for electrically induced structural phase transitions can be observed. These features are common to RFE systems (Lin *et al.*, 2011; Cowley *et al.*, 2011) and would be averaged over by using a stroboscopic measurement.

2. Experimental methods

2.1. PE loop measurement

The PE loop system installed on the beamline uses the Sawyer–Tower measurement method (Sawyer & Tower, 1930), shown in Fig. 1, for two reasons. Firstly, the environment surrounding the automated X-ray diffraction set-up can be electromagnetically noisy because of the many stepper motors that are needed to control the system. This makes detection of small currents very difficult, and it is more convenient to integrate the current on a sense capacitor, giving a degree of immunity to the electromagnetic noise. Secondly, whilst it may normally be possible to shield the sample from the noise by enclosing in a metallic Faraday cage, this is not consistent with the requirement to allow access to the sample for the incident X-ray beam.

The sense capacitor for the Sawyer–Tower method should be made from a low-loss dielectric material such as a poly-

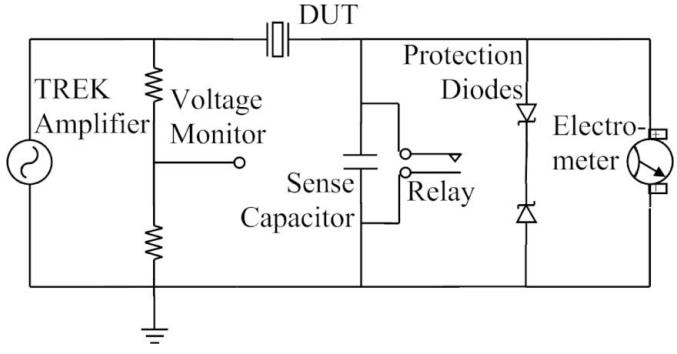

Figure 1
Circuit diagram of the Sawyer–Tower measurement system implemented on the XMaS beamline. The device under test (DUT) is placed in series with a sense capacitor. The voltage across the capacitor is monitored with an electrometer, and compared with the voltage applied to the DUT *via* the monitor voltage output from the amplifier. Back-to-back diodes are placed across the electrometer input for protection in the event of a sample breakdown. The circuit is shorted *via* a relay at the start of each experiment.

propylene, polyester or polyphenylene sulfide. This is particularly important for the lower-frequency measurements, where leakage currents across the capacitor could degrade the results. The size of the capacitor depends on two factors: the capacitance of the device under test (DUT) and the expected polarization of the DUT. An important consideration is that the voltage generated on the sense capacitor should be large enough to be easily measurable, usually greater than a few tens of millivolts, but not so large that it introduces a significant error on the voltage applied across the DUT. The polarization is calculated simply as the product of the sense capacitor capacitance and the electrometer voltage reading, divided by the area of the sample electrodes.

A typical PE loop, after the electric field has been cycled at least once, should be closed, that is the polarization at the end of the cycle should equal the value at the beginning. An open loop can be a result of a real material effect, or due to instrumental factors, such as sense capacitor leakage, DC offsets on the applied voltage or electrometer drift. Resistive leakage from the sample will cause the voltage on the sense capacitor to continuously increase, and so it must be reset periodically by shorting the sense capacitor with the relay. This is also an important factor in keeping the sense capacitor voltage well below the Zener threshold of back-to-back diodes, which protect the electrometer in case of sample breakdown or other short-circuit conditions.

The measured PE loop is dependent on the history of electrical loading on the sample. If the ferroelectric sample has been previously poled in the positive direction, the application of a negative field will cause domain switching, resulting in a large change in P and therefore a loop that is offset vertically from zero. To eliminate such effects, electrical conditioning of the DUT is required. The application of a cyclical electric field with amplitude decreasing over time should produce a gradual depoling of the materials, with a symmetrical polarization response on the next measured cycle.

2.2. XMaS beamline BM28

The XMaS beamline (Paul *et al.*, 1995; Brown *et al.*, 2001) at the ESRF has been designed to perform high-resolution diffraction and magnetic scattering and has been operational since April 1998. The beamline is sited on the soft end of dipole D28, which has a critical energy of 9.8 keV. The primary optics consist of a fixed-exit double-crystal Si(111) monochromator, followed by a toroidal mirror which focuses the beam down to a size of less than 1 mm^2. The experimental hutch is equipped with a six-circle Huber diffractometer that allows scattering in both the vertical and horizontal planes. A comprehensive description of the beamline has been given by Brown *et al.* (2001).

The ferroelectric single crystal is mounted on an insulating substrate of sapphire and Al_2O_3, with electrical connections made to the electroded faces of the crystal perpendicular to the exposed face where the X-ray beam impinges on the crystal. Thermal conductivity and electrical isolation is provided by mounting the crystal on the Al_2O_3 substrate and all electrical leads are wrapped in polytetrafluoroethylene tape (PTFE).

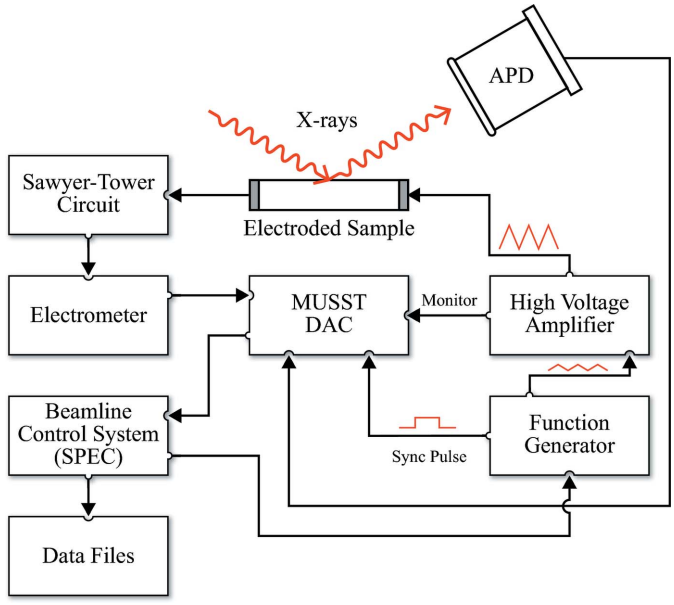

Figure 2
Schematic of the experimental set-up at the XMaS beamline, ESRF. The function generator is used to synchronize and control experimental devices. The fast X-ray detector (APD) scans around the sample in *hkl* space and collects diffraction X-rays. The data are recorded on the ultrafast digital–analogue converter MUSST card at the same time as the electrical data.

The electrical and diffraction set-up is shown in Fig. 2. The electrodes on the crystal are connected to a TREK 610E high-voltage amplifier. A triangular-wave voltage is passed to the amplifier, powered by a function generator which is controlled by the beamline control system. The polarization of the sample in response to the applied field is measured using the Sawyer–Tower method as described in §2.1, and a Keithley 6514 electrometer is used to read out the voltage across the sense capacitor.

2.2.1. Timing of data collection. The diffraction data are recorded as a function of applied electric field, simultaneously with a point detector (avalanche photodiode) at a single point in reciprocal space. The X-ray diffraction data are recorded in real time, synchronized with the polarization, though the diffraction data can be subsequently summed at n points around the E field cycle to improved counting statistics. When carrying out the experiment, n should at a minimum be equal to 20–40 in order to obtain sufficient resolution of the crystallographic changes that occur at the edges of the PE loop, where polarization switching occurs and $\partial P/\partial E$ is greatest.

If high-frequency data are required, many multiple cycles of the PE loop are necessary to collect sufficient integrated X-ray intensity. As such, the method is really only applicable to materials with a repeatable response, and effects such as temperature drift, fatigue or creep are not significant over the timescale of the test. Before calculating a simple average, careful observation of these data is advisable; features such as an overall decline in remanent polarization, or drift of electric field values for phase transitions over time indicate that the

(summed) diffraction data may contain the average patterns of subtly different crystal structures, strains and mosaicity. In contrast to other dynamic measurement studies that utilize stroboscopic data-collection techniques, the real-time data capture in this set-up allows us to identify measurements in which drift or sample changes may affect the analysis of the crystal structure determination.

The beginning few cycles of an example dataset are plotted in Fig. 3. The MUSST (multipurpose unit for synchronization, sequencing and triggering) DAC card forms the heart of this system as it reads the monitor output from the amplifier (applied electric field) and the voltage across the sense capacitor with a sampling rate of up to 40 kHz. It also records the diffraction data and provides the synchronization between the electrical and diffraction data. The change in diffraction intensity shown in the bottom panel is indicative of either peak splitting (owing to structural phase changes) or peak movement from a variation in lattice parameters. The raw data are captured at a set number of points along a line in reciprocal space, and post-processed into an intensity *versus* 2θ plot for each of the n points around the applied voltage cycle. The resultant dataset is a two-dimensional array of diffracted intensity as a function of E field and 2θ. Because the maximum rate of change of 2θ is severely limited by the speed of the stepper motors required to move the detector, it is therefore sensible to cycle the E field variable within each position loop. In this way we can track the E-field-driven evolution of diffraction peaks, at frequencies greater than has been previously possible to measure.

2.2.2. General experimental procedures. To determine the range and direction of scans to be performed in reciprocal space, two-dimensional scans of diffraction peaks of interest are measured at minimum and maximum applied electric fields, an example of which is shown in Fig. 4. Once the range and direction of peak movement has been established, it is possible to choose the slices of the peaks to be recorded during the dynamic experiments, with the assumption that peak shifts at finite frequencies are smaller than or equal to those measured under DC conditions. For crystal structure analysis, the *hkl* scans should be performed along directions of increasing reciprocal lattice wavevector **q**, whereas width measurements of perpendicular cuts through the peaks with an ω scan will provide information on crystal mosaicity and electrically induced strain, through changes in the peak shape rather than position.

In order to mitigate electrical breakdown, dry nitrogen was blown across the sample to eliminate moisture and also oxygen in the vicinity of the sample. Both water and ozone formed from oxygen under the X-ray beam have been shown to provide possible conduction paths across the sample (Weilandics *et al.*, 1987; Kogelschatz *et al.*, 1988).

To probe the dynamic response, the voltage applied to the sample is cycled at each point in reciprocal space to improve diffraction statistics. The data shown in Fig. 3 contained $n = 40$ points around the E field loop, and a typical *hkl* scan was made across the peak in 101 steps. The field was cycled a number of times at each step in reciprocal space to obtain good enough diffraction statistics for crystallographic analysis, the exact number depending on the frequency of the applied field and experimental time constraints. PE data and X-ray diffraction data are recorded continuously, and post-processing of the raw dataset (recorded as a function of time) was employed to sum and normalize X-ray data into n individual intensity–2θ plots.

Whilst the X-ray data are summed and normalized for each point around the PE loop, each individual electrical dataset was studied to ensure the data are consistent throughout the range of the *hkl* scans. RFE samples are sensitive to previous temperature and electrical loading conditions, and effects such as polarization fatigue and relaxation of electrical field values at which structural phase transitions occur may alter peak shape profiles.

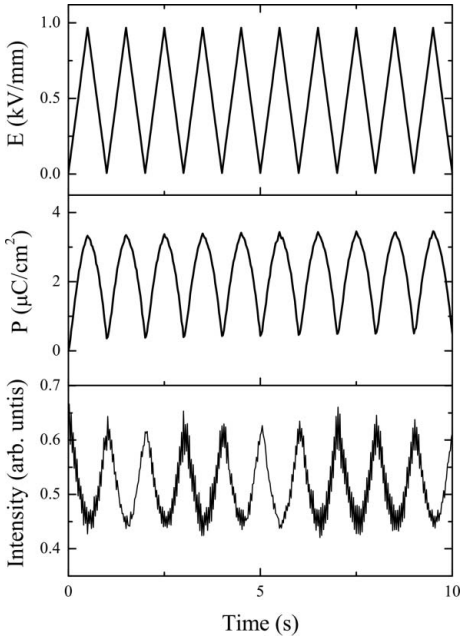

Figure 3
Electric field applied to the sample (top), measured electric polarization (middle) and collected X-ray intensity (bottom) at the 200 peak of a PMN–0.32PT sample plotted as a function of time.

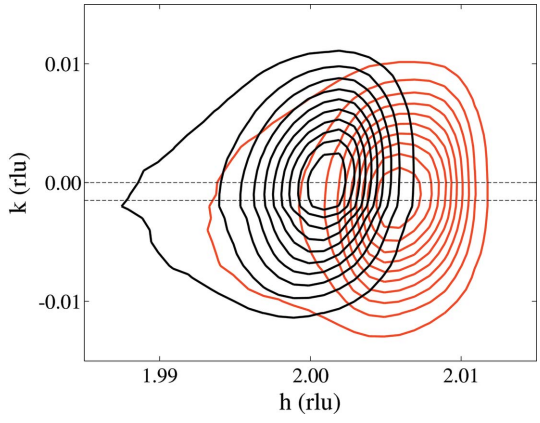

Figure 4
Mesh scan of the 200 peak in PMN–0.32PT at 0 (black) and 1 kV mm^{-1} [grey (red online)] applied electric fields. The black dashed lines indicate directions of *hkl* scans performed during the dynamic experiments.

2.2.3. Results. We have used the XMaS beamline to examine a twinned single crystal of PMN–0.32PT. Electrical contacts were placed on the electroded (100) faces, the beam penetrated the (010) face, and the diffracted X-rays were collected in reflection mode. The crystal was poled along the ⟨100⟩ direction. A triangular-wave electric field was applied to the crystal, and the crystal polarization response was measured; simultaneously reflected intensity data were collected at a point in reciprocal space. This process was repeated at 101 incremental steps along a specified reciprocal lattice direction, identified by the two-dimensional *hk* maps as described in §2.2.2. Reflected intensity data, synchronous to the PE loop measurements, were collected at each applied voltage (from 0 to 1 kV mm^{-1} in 0.05 kV mm^{-1} intervals) at 0.01 Hz, 0.1 Hz and 1 Hz, and at five different temperatures between 298 K and 363 K. The PE loops measured on this sample are unipolar. The extremely high strains produced in these materials as when subjected to repeated cycling of large electric fields means they are likely to crack (Fang *et al.*, 2008) and cause electrical breakdown. Unipolar conditions were therefore chosen to study the electric-field-induced phase switching, whilst maintaining the structural integrity of the sample.

A sample PE loop measurement is plotted in Fig. 5. Whilst there is restricted information present in a unipolar polarization measurement, for example the remanent polarization or coercive electric field is absent, anomalies such as inflection points and changes in gradient may indicate the presence of structural phase changes that can be determined through the analysis of the diffraction data. The evolution of such features can be tracked with changing physical parameters such as temperature, magnetic field and frequency of the applied electric field.

The detailed analysis of how the diffraction and polarization data evolve as a function of frequency and temperature are the subject of a separate future publication. Three diffraction peaks (the pseudo-cubic 200, 220 and 222 reflections) were studied in this experiment. Fig. 6 gives an example dataset on the pseudo-cubic 220 reflection recorded as a function of *E* field cycled at 1 Hz, at a temperature of 298 K. A diffraction pattern was measured at each of the 40 points on a unipolar PE loop. The reflection was then fitted using a published crystal structure models for PMN–0.32PT (Singh *et al.*, 2006). The sample was found to be mixed phase, part monoclinic with space group *Cm* and part tetragonal (*P*4*mm*). This is shown in the figure in blue (*Cm* phase) for the 20$\bar{2}$, 220, 022 and 202 reflections and in red (*P*4*mm* phase) for the 022 and 220 reflections. The dynamic shifts in phase percentage and lattice parameter were then obtained by a constrained refinement over all three reflections with frequency and temperature. The amount of each of the two phases was allowed to refine along with the lattice parameters. To be able to refine the atomic parameters for each phase, a much greater number of reflections would have to be recorded, which was not possible owing to experimental time constraints in this preliminary study.

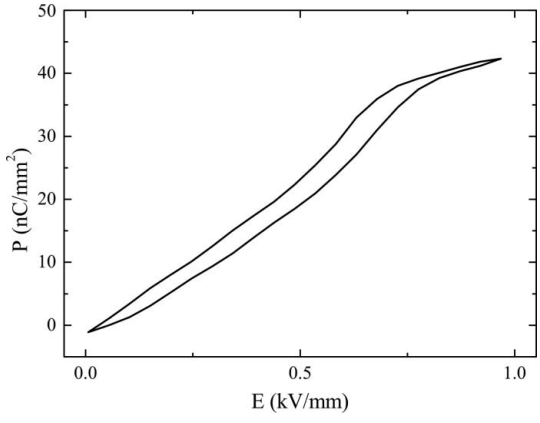

Figure 5
A unipolar PE loop measurement of the PMN–PT single crystal collected at 40 points around the electrical cycle at a frequency of 1 Hz and temperature of 298 K. A change in slope, indicating a change in crystal structure, is evident at an applied field of ∼0.7 kV mm^{-1}.

3. Discussion

This new sample environment enables the determination of the link between electrical polarization characteristics and

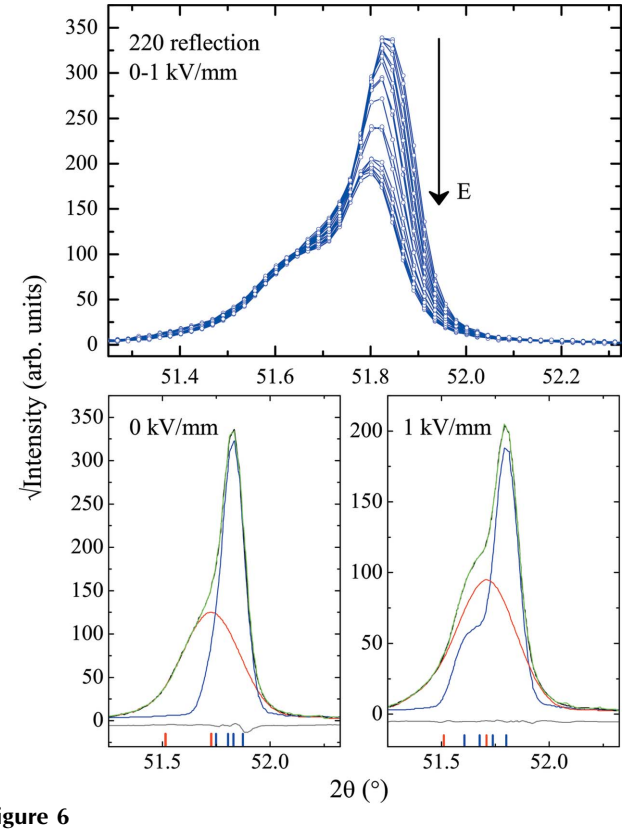

Figure 6
Top panel: intensity–2θ plot of the cubic indexed 220 peak in PMN–0.32PT as a function of applied field from 0 kV mm^{-1} (highest intensity data) to 1 kV mm^{-1} (lowest intensity data) incremented in steps of 0.05 kV mm^{-1}. Bottom panels: peak fitting of the same peak at 0 and 1 kV mm^{-1}. The reflected intensity from the monoclinic phase is plotted in blue, and the tetragonal phase in red, with reflection markers at the bottom of the plot. The total reflected intensity (black) is compared with the fitted model (green) by the difference curve at the bottom in grey.

crystal structure in ferroelectric materials. In the measurement system, real-time diffraction data are collected (though they are later summed as a function of electric field for improved statistics) and so the temporal evolution of the crystal structure can be tracked. The diffracted X-rays are collected at a single point in *hkl*, and so a good knowledge of the zero-field crystal structure, obtained through a previous polycrystalline diffraction experiment, is required before a dynamic experiment can be performed. The information gathered from single-crystal diffraction peaks gives detailed information on the crystal structure composition in the $\theta/2\theta$ direction and orthogonally gives information about the crystal mosaicity or microstructure.

In situ dynamic electric-field neutron and X-ray diffraction experiments have been previously published (Jones *et al.*, 2006; Daniels *et al.*, 2007; Pramanick *et al.*, 2010; Moriyoshi *et al.*, 2011). In all these studies time-resolved diffraction data were collected to measure the lattice strain in response to a square-wave E field, applied to the sample to switch its polarization state. Whilst the electric field was applied *in situ*, none of the studies collected simultaneous polarization data, or macroscopic strain data. These experiments were designed to study the effects of an applied 'on–off' field as a function of time. However, the new measurement system presented here is capable of measuring real-time effects of cyclical electric fields (triangular or sine waves) and the associated evolution of crystallographic parameters.

The results presented in this paper, as a proof-of-concept experiment, were collected at relatively low frequencies when considering the operational requirements of applications such as sonar. The upper limit to such experiments is dictated by the maximum sampling rates of the data acquisition systems at the beamlines (continuously being extended with improvements made in digital data acquisition). With the use of this beamline measurement systems we can directly measure effects such as the dynamics of polarization aging, and the temperature-dependent relaxation-time spectrum, which is typically investigated through techniques such as Brillouin scattering and Raman spectroscopy (Buixaderas *et al.*, 2004).

When performing these experiments, careful consideration should be given to the electrical and temperature history of the sample (Viehland *et al.*, 1992). If the ferroelectric is poled in any particular direction, the measured PE loop will be offset vertically from the origin. In order to centre the charge response, electrical pre-conditioning fields should be applied to the sample before any measurements. Another factor to consider is that temperature cycling through phase transitions in RFE systems is likely to result in a hysteretic crystal response between the first and subsequent temperature cycles, much like the difference in the electrical measurement of the virgin curve of the first and last two quarters of an ideal PE loop response. Therefore, both E field and temperature should be cycled at least three times for consistency of measurement, with careful observation of the PE loop and diffraction data to ensure intensities and polarization values do not continue to drift with increasing electrical or thermal loads.

In the case of piezoelectric materials, small quantities of dopants within the material create cation or anion vacancies in the crystal structure. Dopants are known to result in significant changes in domain structure and electromechanical properties, because they create various types of defects in the crystal structure which have the ability to enhance or inhibit domain wall motion and domain switching. So-called 'soft' piezoelectrics exhibit the largest piezoelectric constants and dielectric permittivities, but suffer from high losses which limit their use in high-frequency applications. 'Hard' piezoelectric materials, on the other hand, can withstand greater excitation levels and frequencies, at the expense of sensitivity and permittivity. The importance of such extrinsic contributions to the piezoelectric response can be characterized by mapping the induced strain and domain size in piezoelectric materials through preferred orientation fitting in Rietveld refinements and/or the FWHM characteristics of peak fitting for single reflections for the single-crystal data (Jones, 2007). In carrying out such analyses as a function of increasing E field and frequency, it should be possible to directly measure the decrease in domain switching associated with relaxation of certain types of domain walls in the material. This has direct implications for applications that benefit from both the intrinsic and extrinsic piezoelectric response, such as actuators, sonar devices and ink-jet printer heads.

4. Conclusions

An *in situ* PE loop measurement system has been integrated into an X-ray diffraction beamline at the ESRF for the determination of the crystallographic response to the application of dynamic electric fields in single-crystal ferroelectric materials. Voltages of up to 10 kV can be applied at a range of frequencies. Initial tests of the systems with PMN–PT samples show that changes in crystallography, such as lattice parameters, phase fractions and peak widths (strain and crystal mosaicity that arise from changes in domain structure), can be correlated to the macroscopic measurement of electrical polarization, details of which are to be presented in a future publication. The X-ray and polarization signals are captured in real time, and stroboscopically summed when post-processing the data. In this work we have developed a new facility that enables the electric-field-induced crystallography in ferroelectric materials to be determined dynamically. Our approach provides synchrotron users with a unique capability for determining the dynamic switching characteristics of ferroelectric materials at cyclical switching (or sub-switching) fields up to 1 kHz, presently. The complex time-dependent origin of the functional properties of relaxor ferroelectrics can now be probed on an atomic (lattice) scale, leading the way for more comprehensive and complete descriptions of the fundamental properties applicable to these industrially relevant materials.

This work was performed on the EPSRC-funded XMaS beamline at the ESRF, directed by M. J. Cooper, C. A. Lucas and T. P. A. Hase. We are grateful to the beamline team of

O. Bikondoa, D. Wermeille and L. Bouchenoire for their invaluable assistance, and to S. Beaufoy and J. Kervin for additional support. Funding was received from the UK's National Measurement System for development of the metrology of the PE loop and integration within the beamline.

References

Bai, F., Wang, N., Li, J., Viehland, D., Gehring, P., Xu, G. & Shirane, G. (2004). *J. Appl. Phys.* **96**, 1620–1627.
Bokov, A. & Ye, Z. (2006). *J. Mater. Sci.* **41**, 31–52.
Brown, S. D., Bouchenoire, L., Bowyer, D., Kervin, J., Laundy, D., Longfield, M. J., Mannix, D., Paul, D. F., Stunault, A., Thompson, P., Cooper, M. J., Lucas, C. A. & Stirling, W. G. (2001). *J. Synchrotron Rad.* **8**, 1172–1181.
Buixaderas, E., Kamba, S. & Petzelt, J. (2004). *Ferroelectrics*, **308**, 131–192.
Chen, K., Zhang, X. & Luo, H. (2002). *J. Phys. Condens. Matter*, **14**, L571–L576.
Cowley, R. A., Gvasaliya, S. N., Lushnikov, S. G., Roessli, B. & Rotaru, G. M. (2011). *Adv. Phys.* **60**, 229–327.
Daniels, J. E., Finlayson, T. R., Davis, M., Damjanovic, D., Studer, A. J., Hoffman, M. & Jones, J. L. (2007). *J. Appl. Phys.* **101**, 104108.
Davis, M. (2007). *J. Electroceram.* **19**, 25–47.
Davis, M., Damjanovic, D. & Setter, N. (2006). *Phys. Rev. B*, **73**, 014115.
Fang, F., Yang, W., Zhang, F. C. & Qing, H. (2008). *J. Mater. Res.* **23**, 3387–3395.
Hinterstein, M., Rouquette, J., Haines, J., Papet, P., Knapp, M., Glaum, J. & Fuess, H. (2011). *Phys. Rev. Lett.* **107**, 077602.
Jones, J. (2007). *J. Electroceram.* **19**, 69–81.
Jones, J. L., Hoffman, M., Daniels, J. E. & Studer, A. J. (2006). *Appl. Phys. Lett.* **89**, 092901.
Kogelschatz, U., Eliasson, B. & Hirth, M. (1988). *Ozone Sci. Eng.* **10**, 367–378.
Lin, D., Li, Z., Cheng, Z.-Y., Xu, Z. & Yao, X. (2011). *Solid State Commun.* **151**, 1188–1191.
McLaughlin, E. A., Liu, T. & Lynch, C. S. (2004). *Acta Mater.* **52**, 3849–3857.
Moriyoshi, C., Hiramoto, S., Ohkubo, H., Kuroiwa, Y., Osawa, H., Sugimoto, K., Kimura, S., Takata, M., Kitanaka, Y., Noguchi, Y. & Miyayama, M. (2011). *Jpn. J. Appl. Phys.* **50**, 09NE05.
Park, S. & Hackenberger, W. (2002). *Curr. Opin. Solid State Mater. Sci.* **6**, 11–18.
Park, S. & Shrout, T. (1997). *J. Appl. Phys.* **82**, 1804–1811.
Paul, D., Cooper, M. & Stirling, W. (1995). *Rev. Sci. Instrum.* **66**, 1741–1744.
Pramanick, A., Prewitt, A. D., Cottrell, M. A., Lee, W., Studer, A. J., An, K., Hubbard, C. R. & Jones, J. L. (2010). *Appl. Phys. A*, **99**, 557–564.
Sawyer, C. & Tower, C. (1930). *Phys. Rev.* **35**, 269.
Schonau, K. A., Knapp, M., Kungl, H., Hoffmann, M. J. & Fuess, H. (2007). *Phys. Rev. B*, **76**, 144112.
Singh, A. K., Pandey, D. & Zaharko, O. (2006). *Phys. Rev. B*, **74**, 024101.
Viehland, D., Li, J., Jang, S., Cross, L. & Wuttig, M. (1992). *Phys. Rev. B*, **46**, 8013–8017.
Waser, R., Bottger, U. & Tiedke, S. (2005). Editors. *Polar Oxides Properties, Characterization and Imaging.* Weinheim: Wiley-VCH.
Weilandics, C., Rohrig, N. & Gmur, N. F. (1987). *Ozone Production at the National Synchotron Light Source*, Technical Report. National Synchrotron Light Source, Brookhaven National Laboratory, Upton, NY, USA.
Ye, Z., Bing, Y., Gao, J., Bokov, A., Stephens, P., Noheda, B. & Shirane, G. (2003). *Phys. Rev. B*, **67**, 104104.
Ye, Z. & Dong, M. (2000). *J. Appl. Phys.* **87**, 2312–2319.
Zhao, X., Fang, B., Cao, H., Guo, Y. & Luo, H. (2002). *Mater. Sci. Eng. B*, **96**, 254–262.